INSTITUTE OF PHYSICS PUBLISHING JOURNAL OF PHYSICS: CONDENSED MATTER

J. Phys.: Condens. Matter **15** (2003) 1223–1233 PII: S0953-8984(03)53126-5

Structural and electrical properties of *c*-axis epitaxial and polycrystalline $Sr_3Bi_4Ti_6O_{21}$ thin films

S T Zhang[1], Y F Chen[1], H P Sun[2], X Q Pan[2], W S Tan[3], Z G Liu[1] and N B Ming[1]

[1] National Laboratory of Solid State Microstructures and Department of Materials Science and Engineering, Nanjing University, Nanjing 210093, China
[2] Department of Materials Science and Engineering, The University of Michigan, Ann Arbor, MI 48109-2136, USA
[3] National Laboratory of Solid State Microstructures and Department of Physics, Nanjing University, Nanjing 210093, China

Received 6 September 2002, in final form 29 November 2002
Published 17 February 2003
Online at stacks.iop.org/JPhysCM/15/1223

Abstract

c-axis epitaxial and polycrystalline $Sr_3Bi_4Ti_6O_{21}$ (SBTi) thin films were fabricated on (001)$SrTiO_3$ (STO) single-crystal substrates and Pt/Ti_2/SiO_2/Si substrates respectively, by pulsed laser deposition (PLD). Structures of the films were systematically characterized by x-ray diffraction (XRD), including θ–2θ-scans, rocking curve scans and ϕ-scans, atomic force microscopy and transmission electron microscopy (TEM). The epitaxial orientation relation of the SBTi films on STO is established by selected-area electron diffraction and XRD ϕ-scans to be (001)SBTi ∥ (001)STO, $[1\bar{1}0]$SBTi ∥ [010]STO. Cross-sectional high-resolution TEM studies on the epitaxial SBTi film revealed that SBTi is a single-phase material. A special kind of irrational atomic shift along the [001] direction was observed and is discussed in detail. By using an evanescent microwave probe (EMP), the room-temperature dielectric constant of the epitaxial SBTi film was measured to be 211 ± 20. Excellent electrical properties of the polycrystalline SBTi films with Pt bottom and top electrodes were exhibited: the P_r and E_c values were 4.1 μC cm^{-2} and 75 kV cm^{-1} respectively, the nonvolatile polarizations decreased by less than 5% after 2.22×10^9 switching cycles and the dielectric constant and loss tangent were 363 and 0.04 at 100 kHz.

1. Introduction

Recently, Bi-layered oxide (Aurivillius phases) ferroelectric thin films have been intensively studied for scientific interest and in view of technical applications in nonvolatile ferroelectric random access memory (NVFRAM) due to their structural anisotropy and low coercive field and leakage current, long retention, minimal tendency to imprint and little fatigue with the usual

Pt electrode [1]. The Bi-layered oxide family can be described as $(Bi_2O_2)^{2+}(A_{m-1}B_mO_{3m+1})^{2-}$, where A represents Bi, Ba, Pb, Sr, Ca, K, Na and rare earth elements, B represents Ti, Ta, Nb, W, Mo, Fe etc and m represents the number of BO_6 octahedra between two neighbouring Bi_2O_2 layers. For example, $SrBi_2Ta_2O_9$ and $SrBi_2Nb_2O_9$ ($m = 2$), $Bi_4Ti_3O_{12}$ ($m = 3$), $SrBi_4Ti_4O_{15}$ ($m = 4$) and $Sr_2Bi_4Ti_5O_{18}$ ($m = 5$) have two, three, four and five octahedra respectively. Structural and electrical properties of these materials in the form of thin films have been well studied [1–7]. On the other hand, it is reported that the synthesis of a homologous oxide thin-film system can offer tremendous potential for tailoring the ferroelectric and dielectric properties of materials. For example, by preparing the first five members of the $Sr_{n+1}Ti_nO_{3n+1}$ Ruddlesden–Popper homologous series by molecular beam epitaxy (MBE), Haeni *et al* revealed that the first member of this series, Sr_2TiO_4, has several potential advantages over the $n = \infty$ member, $SrTiO_3$ (STO), in the applications of metal–oxide–semiconductor field effect transistors (MOSFETs) [8]. Therefore, in the case of the Bi-layered oxide family, it is of great interest to investigate the structural and electrical properties of $Sr_3Bi_4Ti_6O_{21}$ (SBTi), which is a member of the family with six octahedra between two neighbouring Bi_2O_2 layers.

It is suggested that Bi-layered oxides with $m \geqslant 6$ cannot occur naturally and some attempts to fabricate such an oxide ended in a mixture of the phase $Sr_2Bi_4Ti_5O_{18}$ and STO [9]; however, there is no direct reason to prohibit their occurrence, especially in the form of a thin film. Although optical properties of SBTi film have been reported [10], no careful structural characterization (i.e. cross-sectional high-resolution transmission electron microscopy (HRTEM)) has been done to ensure it is really a single-phase material. To meet this goal, an HRTEM study of SBTi thin film is necessary.

From the viewpoint of application, the growth of non-c-axis oriented Bi-layered oxide films are of particular significance because their properties dramatically depend on their orientation. However, probing c-axis oriented films is important for understanding the basic structure–property relations [11].

In this paper, c-axis-epitaxial SBTi thin films were prepared on (001)STO single-crystal substrates by pulsed laser deposition (PLD). Cross-sectional HRTEM studies revealed that SBTi is really a single-phase material. For comparison, polycrystalline SBTi films were prepared on $Pt/TiO_2/SiO_2/Si$ substrates by PLD and their electrical properties were briefly reported.

2. Experimental procedure

For Bi-layered oxides, the pseudo-tetragonal or the orthorhombic structure can be used [12]. In the case of pseudo-tetragonal structure, the a and b lattice constants of SBTi are assumed to be about 3.84 Å, which is very close to the lattice constant of cubic STO ($a = 3.90$ Å) and that of pseudo-cubic $LaAlO_3$ (LAO, $a = 3.79$ Å). The lattice mismatches are about 1.5% between this material and STO and about 1.6% between this material and LAO; therefore, STO and LAO are promising substrates for the growth of c-axis epitaxial SBTi thin films. In the present paper, however, orthorhombic structure indexing will be used.

The SBTi pellets used as the PLD target were prepared by solid-state reaction with starting materials $SrCO_3$, Bi_2O_3 (in excess of the stoichiometric requirement by 20 mol% initially because of the volatility) and TiO_2. The mixture of $SrCO_3$, Bi_2O_3 and TiO_2 with the ratio of Sr:Bi:Ti = 3:4.8:6 was ball milled for 12 h, preheated at 700 °C for 2 h and pressed into pellets; these pellets were then fired at 1050 °C for 2 h.

The PLD processes were performed using a Lambda Physik LPX205i KrF excimer laser system with 248 nm radiation and 30 ns pulse width. A pellet was placed in the deposition chamber and a pulsed laser beam with a repetition rate of 5 Hz was focused on the rotated

pellet. At 750 °C, SBTi thin films were prepared on (001)STO and Pt/TiO_2/SiO_2/Si substrates for 20 min under a flowing oxygen partial pressure of 30 Pa, respectively. After each deposition, the film was *in situ* annealed at 750 °C for 10 min under 0.5 atm oxygen pressure. For electrical measurements, Pt top electrodes 200 μm in diameter were deposited onto the surface of the SBTi/Pt/TiO_2/SiO_2/Si (referred to as SBTi/Pt) through a shadow mask at room temperature. Finally, the Pt/SBTi/Pt capacitors were post-annealed at 750 °C for 30 min under 0.5 atm oxygen pressure.

Crystal structures of the films were characterized by x-ray diffraction (XRD), including θ–2θ-scans, rocking curve scans (using a Rigaku x-ray diffractometer with nickel filtered Cu Kα radiation) and ϕ-scans (using a Siemens D5000 x-ray diffractometer). A Nanoscope IIIa atomic force microscope (AFM) from Digital Instruments was used to record the surface morphology. The cross-sectional microstructure of the SBTi/STO heterostructure was examined by HRTEM using a JEOL 4000EX electron microscope operated at 400 kV. The room-temperature dielectric constant (ϵ) of the epitaxial SBTi film was measured by using an evanescent microwave probe (EMP) while ferroelectric and dielectric properties of the polycrystalline SBTi film with Pt top and bottom electrodes were measured by using an RT6000HVS ferroelectric tester (Radiant Technologies) and an HP 4294A impedance/phase analyser.

3. Structural and dielectric properties of SBTi films on (001)STO single-crystal substrates

3.1. XRD pattern

Figure 1 shows the typical XRD θ–2θ scan pattern of an SBTi film on a (001)STO single-crystal substrate. The peaks were indexed using orthorhombic structure by assuming $a \approx b = 5.43$ Å and $c \approx 57.00$ Å [10]. Obviously, only (00$\underline{2l}$) peaks of SBTi and (00l) peaks of STO substrate can be detected, which is consistent with the other report [10]. This result indicates that the film is highly c-axis oriented. To detect if there is a tilt of c-axis orientation away from the surface normal, rocking curve experiments were performed. The rocking curve scans of the STO (001) reflection and the SBTi (00$\underline{14}$) reflection are shown in figures 2(a) and (b), respectively. The full width at half maximum (FWHM) of STO (001) and SBTi (00$\underline{14}$) reflections are 0.2° and 1.0°, respectively. The larger FWHM of the SBTi (00$\underline{14}$) reflection than that of the STO (001) reflection might result from the fact that, although the SBTi film is highly c-axis oriented, compared with the STO single crystal, the c-axis-orientation quality of the SBTi film is not as good as the STO single crystal.

X-ray ϕ-scans were performed to determine the epitaxial nature of the SBTi film on STO substrate. In the ϕ-scan measurements, the (102) reflection of STO and the (11$\underline{13}$) reflection of SBTi were selected. When 2θ and ψ, the tilt angle off the surface normal, were fixed at 31.04° and 48.44°, respectively, the (11$\underline{13}$) plane ϕ-scan result of the SBTi film was obtained by rotating the sample through 0°–360°. This result is plotted in figure 3(a). Then with fixed 2θ and ψ of 52.34° and 26.57°, respectively, the (102) plane ϕ-scan result of the single-crystal STO substrate could also be obtained by rotating the sample through 0°–360°, as plotted in figure 3(b). The measured FWHM of the (11$\underline{13}$) reflection of SBTi and the (102) reflection of STO is 0.5° and 0.1°, respectively. In figure 3(b), four equally spaced peaks separated by 90° could be observed, as was expected for cubic STO. In the case of figure 3(a), four peaks separated by about 90° indicate that the c-axis is the fourfold symmetric axis of the SBTi film. The in-plane lattice of SBTi is believed to be completely restricted by the substrate lattice, to form a pseudomorphic tetragonal structure without orthogonal distortion [13]. It should be noted that the peaks of SBTi at about 160° and 250° showed a small shift with respect to the

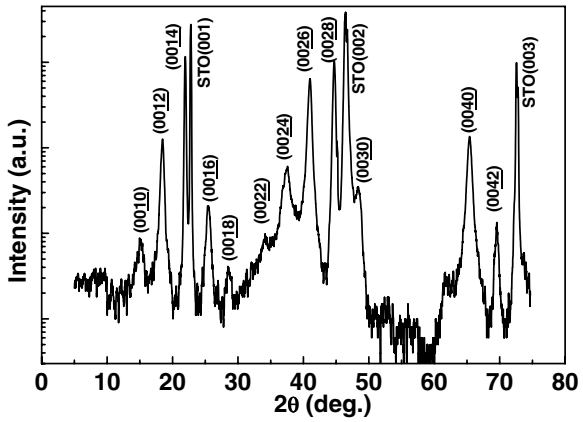

Figure 1. The typical XRD pattern of an SBTi thin film deposited on a (001)STO single-crystal substrate.

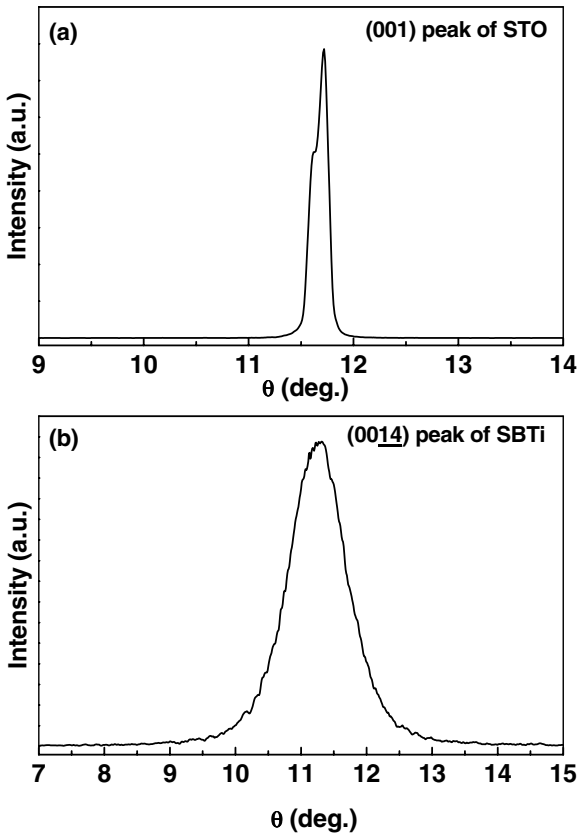

Figure 2. Rocking curves of (a) the (001) reflection of STO and (b) the (00$\underline{14}$) reflection of SBTi, showing high *c*-axis-orientation quality of SBTi films on STO.

corresponding peaks of STO. This might result from the fact that the *a*- and *b*-lattice constants of pseudomorphic tetragonal SBTi are not strictly equal. The angle between (102) of STO and (11$\underline{13}$) of SBTi is 0°, which is almost equal to the calculated value. From this, the alignment of

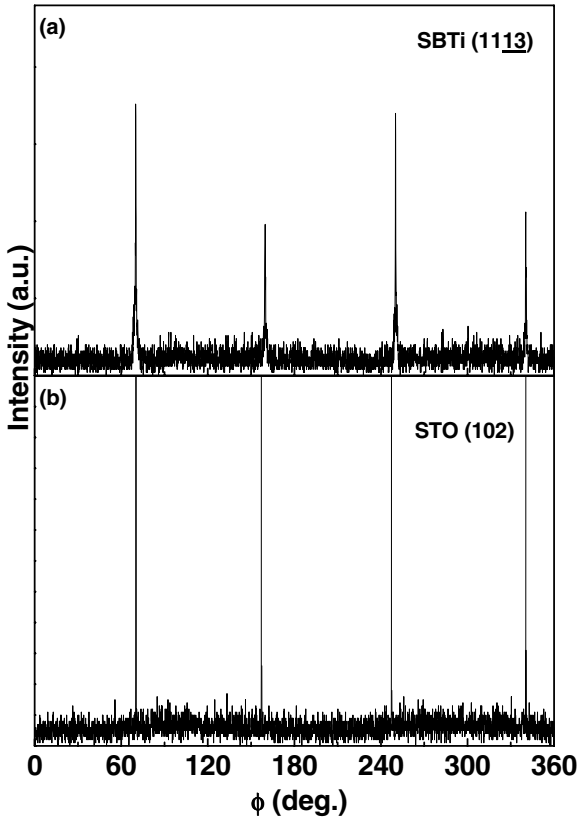

Figure 3. The x-ray ϕ-scans of SBTi/STO (a) for the (11$\underline{13}$) reflection of SBTi and (b) for the (102) reflection of STO.

the in-plane lattice vectors can be concluded. The x-ray ϕ-scan results confirmed that the SBTi film was epitaxially grown on STO single-crystal substrate with the epitaxial arrangements of (001)SBTi ∥ (001)STO, [110]SBTi ∥ [100]STO and [1$\bar{1}$0]SBTi ∥ [010]STO.

3.2. AFM surface morphology

The surface morphology of the *c*-axis epitaxial SBTi film on STO was recorded by an AFM, as shown in figure 4. Over an area of 3 μm × 3 μm, a relatively rough surface with some random islands was shown. This indicates that the SBTi films were of island-like growth, as will be discussed in the following.

3.3. Cross-sectional TEM study

Figure 5(a) shows a typical [010] zone axis selected-area electron diffraction (SAED) pattern of the single-crystal STO substrate. Figure 5(b) is the SAED pattern taken from the SBTi film and figure 5(c) is the SAED pattern taken in the area covering both the films and the substrate. Figure 5(b) is identified to be the [1$\bar{1}$0] zone electron diffraction pattern of the SBTi structure. Figure 5(c) shows the mixing SAED pattern of [010] STO and [1$\bar{1}$0] SBTi, because besides the electron diffraction pattern of SBTi, that of STO, for example, [100] of STO indicated by the arrow, can also be identified. From these SAED patterns, the following epitaxy relation

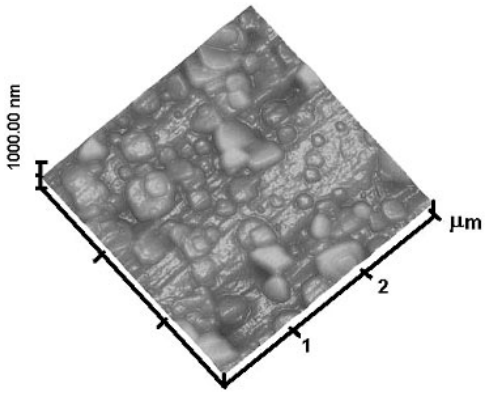

Figure 4. The typical three-dimensional AFM surface morphology of SBTi thin film on STO substrate.

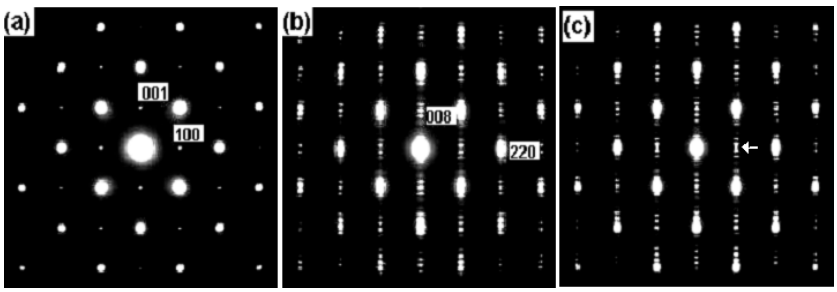

Figure 5. The typical SAED pattern of (a) the [010] zone of the STO, (b) the [$1\bar{1}0$] zone of SBTi6 and (c) the interface between STO and SBTi6, respectively.

is established: (001)SBTi ‖ (001)STO, [$1\bar{1}0$]SBTi ‖ [010]STO, which is consistent with the x-ray ϕ-scan results.

The low-magnification cross-sectional TEM overview of the *c*-axis epitaxial SBTi film on STO is shown in figure 6(a). It emphasizes that the individual SBTi grains extend from the bottom to the top surface. The mean thickness of the SBTi film is determined to be 500 nm. In figure 6(b), the film shows a number of wedge shaped contrasts parallel to the (001) plane of the substrate surface, which should be attributed to the large *c*-axis lattice constant, i.e., layered structure is obtained. In an enlarged image area (figure 6(c)), there are obvious overall staircase-like irrational shifts of both Bi_2O_2 perovskite units along the [001] direction. This may result from the following mechanism. As indicated by the AFM surface morphology (figure 4) and the low-magnification cross-sectional TEM image (figure 6(a)), the SBTi films were of island-like growth. Therefore, it is reasonable that at the early stage of the film growth, each epitaxial island grain is separate from the neighbouring ones. Generally, the growth rate of each grain is different. As a result, when the neighbouring grains come into contact with each other, the Bi_2O_2/perovskite/Bi_2O_2 atomic sequence may not be identical, which is expected to be responsible for the observed atomic shift. In figure 6(c), another slight atomic tilting can be seen, as indicated by the white arrow, which is intrinsic to the Bi-layered perovskite oxides [14]. It is reported that the TiO_6 octahedra can tilt along the four nominally equivalent *a*-axes [15]; this tilting will lead to the atoms such as Ti bending upward, downward, backward or forward randomly. In figure 6(c), the arrow indicates such a tilting resulting from the backward or

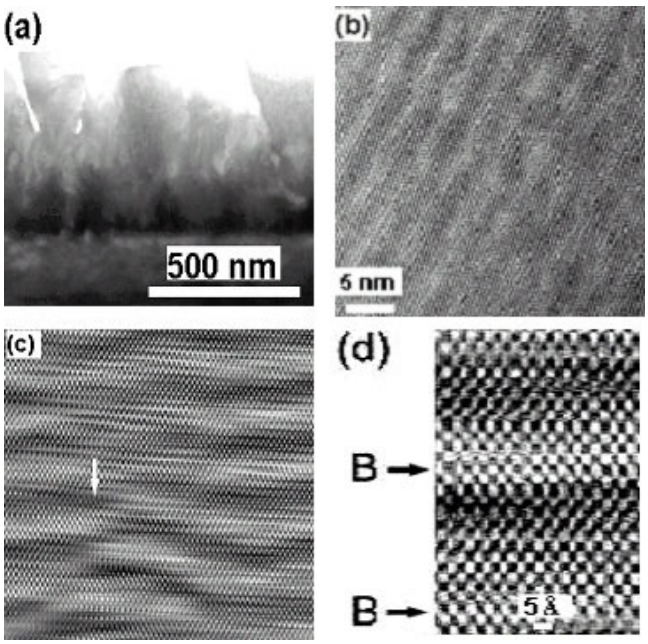

Figure 6. Cross-sectional high-resolution TEM images of (a) overview of SBTi/STO, (b)–(d) enlarged high-resolution TEM images of the epitaxial SBTi film, respectively.

forward bend of TiO_6 octahedra (perpendicular to the paper). Figure 6(d) is the local HRTEM image of SBTi. The layered structure can be seen clearly. The spots corresponding to the Sr and Ti columns have relatively low intensities, the Bi columns high intensities, while O columns are not seen. This is because of their different atomic numbers: $Z = 38$, 22, 83 and 8 for Sr, Ti, Bi and O, respectively. The Sr and Ti columns have little difference in intensity because of their close atomic numbers. The stacking blocks of the alternate Bi_2O_2 layers and Bi–Ti–O/Sr–Ti–O perovskite layers are indicated by letters B where the perovskite blocks lie between two neighbouring (Bi_2O_2) layers. It should be noted that between double Bi_2O_2 layers, there are other Bi columns that can be detected, which correspond to the Bi–Ti–O ferroelectric blocks. The measured *c*-axis lattice constant is 5.670 nm. Some intergrowth is observed in localized regions. In fact, intergrowth can be seen in other Bi-layered oxide films, such as SBT and SBN [16]. It is suggested that the Bi content affected by growth conditions must be responsible for the intergrowth of Bi-layered oxide films [16].

3.4. Dielectric property

The growth of the *c*-axis epitaxial films allows the dielectric constant (ϵ) of this highly anisotropic material to be measured. ϵ of the epitaxial film on STO substrate was measured by an EMP [8, 17, 18] to be 211 ± 20. This is comparable to the EMP result measured on the *c*-axis epitaxial SBTi film on LAO single-crystal substrate and the result measured on *c*-axis epitaxial SBTi film in a parallel plate capacitor structure ($LaNiO_3$/SBTi/$LaNiO_3$/$LaAlO_3$) with an HP4294A impedance/phase analyser, which will be published elsewhere. However, ϵ of the *c*-axis epitaxial SBTi film is much lower than that of the polycrystalline SBTi film measured in parallel plate capacitor structure (Pt/SBTi/Pt/TiO_2/SiO_2/Si) with an HP4294A, which will be shown and discussed in the following.

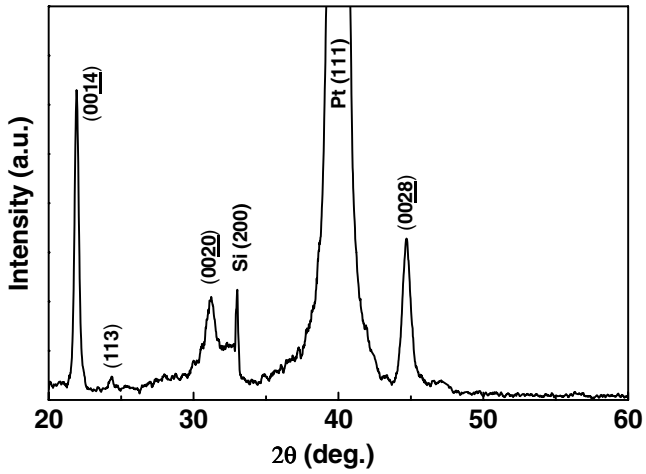

Figure 7. The XRD pattern of SBTi thin film deposited on Pt/SBTi/Pt/TiO_2/Si_2/Si substrate.

4. Structural and electrical properties of polycrystalline SBTi films on Pt-coated Si substrates

4.1. XRD pattern

Figure 7 shows a typical XRD pattern of the SBTi film deposited on Pt/TiO_2/SiO_2/Si substrate. It should be noted that no peaks of STO could be detected in the XRD pattern, indicating that the films were not a mixture of $Sr_2Bi_4Ti_5O_{18}$ and STO phases. The FWHM of the (00$\underline{14}$) peak was 0.25°. The sharp peaks in this XRD pattern suggested the films are well crystallized. The average grain size in the SBTi films was estimated to be about 34 nm, using the Scherrer equation.

4.2. Ferroelectric properties

Typical hysteresis loops of the Pt/SBTi/Pt/TiO_2/SiO_2/Si capacitor are shown in figure 8. At an applied field of about 180 kV cm^{-1}, the remnant polarization (P_r) and coercive field (E_c) values were 1.3 μC cm^{-2} and 34 kV cm^{-1} respectively. With the field increased to about 400 kV cm^{-1}, a well saturated loop was obtained and P_r and E_c were 4.1 μC cm^{-2} and 75 kV cm^{-1} respectively. The relatively small P_r value might result from the fact that the films were highly *c*-axis oriented: it is well known that Bi-layered ferroelectric oxides have the polarization vectors in *a*–*b*-planes. Other highly *c*-axis oriented Bi-layered oxide (such as $BaBi_4Ti_4O_{15}$) thin films also showed such a hysteresis loop with small P_r [19]. This observation confirmed that the P_r of a Bi-layered oxide film depends greatly on film orientation.

Fatigue tests were carried out by applying bipolar pulses about 267 kV cm^{-1} (12 V) in amplitude and 50 kHz in frequency to a Pt/SBTi/Pt/TiO_2/SiO_2/Si capacitor. A typical fatigue characteristic is shown in figure 9. It can be seen that after 2.2×10^{-9} switching cycles, the values of positive nonvolatile polarization decreased from 1.40 to 1.38 μC cm^{-2} and the values of negative nonvolatile polarization decreased from 1.44 to 1.37 μC cm^{-2}. This means that the film retained at least 95% of its initial polarization. It has been suggested that most of the domain configuration in Bi-layered oxides should be the 180° domains [20]. The excellent fatigue property of SBTi thin films may be due to the 180° domains and the small polarization:

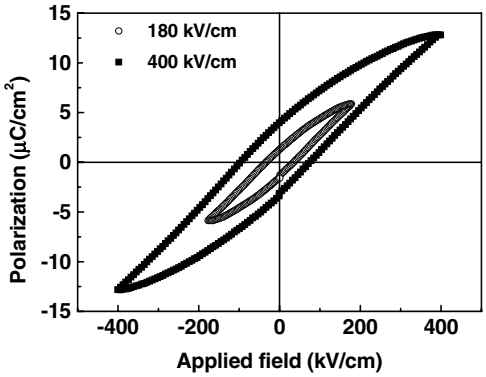

Figure 8. The P–E hysteresis loops of the Pt/SBTi/Pt/TiO_2/Si_2/Si capacitor.

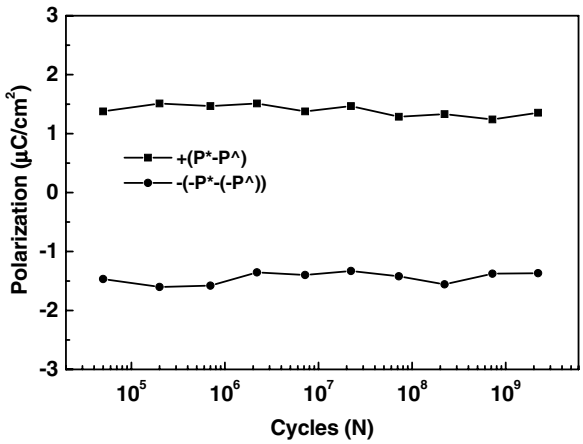

Figure 9. The fatigue characteristics of the Pt/SBTi/Pt/TiO_2/Si_2/Si capacitor.

charges trapped at such a domain boundary can be easily detrapped and small polarization can reduce trap depth for charges at domain boundary. These will result in less trapped charge and lower domain pinning rate, thus good fatigue characteristics [21].

4.3. Dielectric properties

Figure 10 shows the result of ϵ and loss tangent ($\tan\delta$) of the Pt/SBTi/Pt/TiO_2/SiO_2/Si capacitor as a function of frequency. Generally, no severe dispersion was observed. At about 100 kHz, the measured ϵ and $\tan\delta$ were 363 and 0.04 respectively. As the frequency was scanned to 2 MHz, the ϵ dropped to 347, about a 6% decrease of the initial value. The $\tan\delta$ remained fairly low (about 0.04–0.07) in the frequency range mentioned above. It is well known that the spontaneous polarization of these Bi-layered oxides is along the a-axis [22]; therefore, the larger ϵ along the a-axis than that along the c-axis is reasonable. In fact, this result has also been revealed in $SrBi_2Ta_2O_9$, another Bi-layered oxide [23]. In the case of polycrystal SBTi film, both a- and c-axis-oriented grains have contributions to the ϵ value. Therefore, the ϵ of the polycrystalline SBTi film is larger that that of the c-axis epitaxial SBTi film.

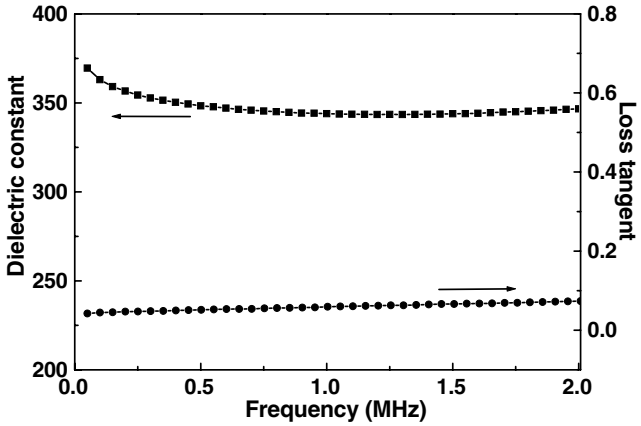

Figure 10. Frequency dependence of dielectric constant and loss tangent of the Pt/SBTi/Pt/TiO_2/Si_2/Si capacitor.

5. Conclusions

Bi-layered SBTi films were fabricated on (001)STO single-crystal substrates and Pt/TiO_2/SiO_2/Si substrates respectively by PLD. XRD and HRTEM measurements confirmed that the SBTi is really a single-phase material. The epitaxial relation of the SBTi film on STO was established to be (001)SBTi ∥ (001)STO, [1$\bar{1}$0]SBTi ∥ [010]STO, by SEAD and XRD ϕ-scans. A special kind of atomic shift along the c-axis and a local slight tilting of TiO_6 octahedra, which is intrinsic to Bi-layered oxides, were observed and discussed. The dielectric constant of the epitaxial SBTi films was measured to be 211 ± 20 by EMP. Based on the existence of single-phase SBTi, electrical properties of polycrystalline SBTi films with Pt bottom and top electrodes were examined. The measured P_r and E_c were 4.1 μC cm^{-2} and 75 kV cm^{-1}, respectively. Excellent fatigue-free property up to 2.2×10^9 switching cycles was experimentally shown. The dielectric constant and loss tangent of the polycrystalline films were 363 and 0.04 at 100 kHz.

Acknowledgments

The authors would like to acknowledge discussion with and support from Dr X-D Xiang and Dr G Wang in the EMP measurements. The work at the Nanjing University was jointly supported by the State Key Program for Basic Research of China and the National Nature Science Foundation of China (No 50225204). The work at the University of Michigan was supported by the National Science Foundation through grant DMR 9875405 (CAREER, XQP) and DMR/IMR 9704175.

References

[1] Paz de Araujo C A, Cuchlaro J D, McMillan L D, Scott M C and Scott J F 1995 *Nature* **374** 627
[2] Shimakawa Y, Kubo Y, Kamiyama T, Asano H and Izumi F 1999 *Appl. Phys. Lett.* **74** 1904
[3] Gruverman A, Pignolet A, Satyalakshmi K M, Alexe M, Zakharov N D and Hesse D 2000 *Appl. Phys. Lett.* **76** 106
[4] Al-Shareef H N, Dimos D, Boyle T J, Warren W L and Tuttle B A 1996 *Appl. Phys. Lett.* **68** 690
[5] Joshi P C and Krupanidhi S B 1993 *Appl. Phys. Lett.* **62** 1928

[6] Irie H and Miyayama M 2001 *Appl. Phys. Lett.* **79** 251
[7] Zhang S T, Xiao C S, Fang A A, Yang B, Sun B, Chen Y F, Liu Z G and Ming N B 2000 *Appl. Phys. Lett.* **76** 3112
[8] Haeni J H, Theis C D, Schlom D G, Tian W, Pan X Q, Chang H, Takeuchi I and Xiang X D 2001 *Appl. Phys. Lett.* **78** 3292
[9] Aurivillius B and Fang P H 1962 *Phys. Rev.* **126** 893
[10] Tachiki M, Yamamuro K and Kobayashi T 1996 *Japan. J. Appl. Phys.* **35** L719
[11] Yan Y, Al-Jassim M M, Xu Z, Lu X, Diehland D, Payne M and Pennycook S J 1999 *Appl. Phys. Lett.* **75** 1961
[12] Hesse D, Zakharov N D, Pignolet A, James A R and Senz S 2000 *Cryst. Res. Technol.* **35** 641
[13] Suzuki T, Nishi Y, Fujimoto M, Ishikawa K and Funakubo H 1999 *Japan. J. Appl. Phys.* **38** L1262
[14] Scott J F 2000 *Ferroelectric Memories* (Berlin: Springer) p 68
[15] Srolovitz D J and Scott J F 1986 *Phys. Rev.* B **34** 1815
[16] Duclere J R, Guilloux-Viry M, Perrin A, Laval J Y and Dubon A 2002 *Appl. Surf. Sci.* **186** 391
[17] Gao C and Xiang X D 1998 *Rev. Sci. Instrum.* **69** 3846
[18] Chang H, Takeuchi I and Xiang X D 1999 *Appl. Phys. Lett.* **74** 1165
[19] Satyalakshmi K M, Alexe M, Pignolet A, Zakharov N D, Hamagea C, Senz S and Hesse D 1999 *Appl. Phys. Lett.* **74** 603
[20] Li T, Zhu Y, Desu S B, Peng C H and Nagata M 1996 *Appl. Phys. Lett.* **68** 616
[21] Dimos D, Al-Shareef H N, Warren W L and Tuttle B A 1682 *J. Appl. Phys.* **80**
[22] Withers R L, Thompson J G and Rae A D 1991 *J. Solid State Chem.* **94** 404
[23] Lee H N, Visinoiu A, Senz S, Harnagea C, Pignolet A, Hesse D and Gosele U 2000 *J. Appl. Phys.* **88** 6658